Dalton Transactions

An international journal of inorganic chemistry

rsc.li/dalton

ROYAL SOCIETY
OF CHEMISTRY
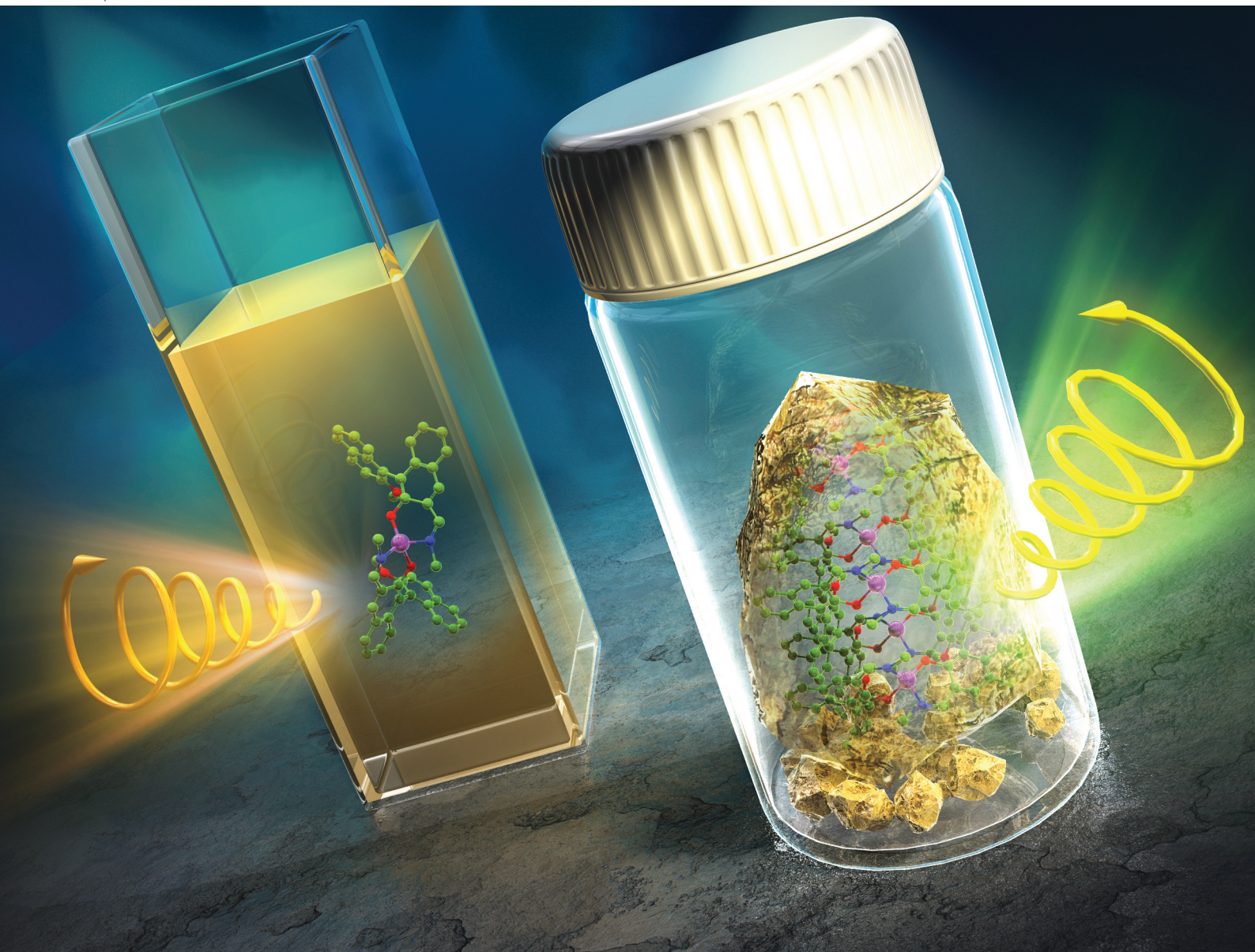
PAPER
Hiroyuki Nishikawa *et al.*
Aggregation-induced enhanced fluorescence emission of
chiral Zn(ɪɪ) complexes coordinated by Schiff-base type
binaphthyl ligands

Check for updates

Aggregation-induced enhanced fluorescence emission of chiral Zn(II) complexes coordinated by Schiff-base type binaphthyl ligands†

Daiki Tauchi,[a] Katsuya Kanno,[a] Masashi Hasegawa, [ID][b] Yasuhiro Mazaki,[b]
Kazunori Tsubaki, [ID][c] Ken-ichi Sugiura,[d] Takuya Shiga,[e] Seiji Mori [ID][a] and
Hiroyuki Nishikawa [ID] *[a]

A pair of novel chiral Zn(II) complexes coordinated by Schiff-base type ligands derived from BINOL (1,1′-bi-2-naphthol), **R-/S-Zn**, were synthesized. X-ray crystallography revealed the presence of two crystallographically independent complexes; one has a distorted trigonal–bipyramidal structure coordinated by two binaphthyl ligands and one disordered methanol molecule (molecule A), while the other has a distorted tetrahedral structure coordinated by two binaphthyl ligands (molecule B). Numerous CH···π and CH···O interactions were identified, contributing to the formation of a 3-dimensional rigid network structure. Both **R-/S-Zn** exhibited fluorescence in both CH_2Cl_2 solutions and powder samples, with the photoluminescence quantum yields (PLQYs) of powder samples being twice as large as those in solutions, indicating aggregation-induced enhanced emission (AIEE). The AIEE properties were attributed to the restraint of the molecular motion arising from the 3-dimensional intermolecular interactions. CD and CPL spectra were observed for **R-/S-Zn** in both solutions and powders. The dissymmetry factors, g_{abs} and g_{CPL} values, were within the order of 10^{-3} to 10^{-4} magnitudes, comparable to those reported for chiral Zn(II) complexes in previous studies.

Introduction

Circularly polarized organic light-emitting diodes (CP-OLEDs) have attracted extensive attention owing to their potential utility in advanced fields such as display technology, optical information communication, chemical and biological sensors, and so on.[1,2] The fabrication of CP-OLEDs necessitates chiral luminescent materials exhibiting a substantial degree of circularly polarized luminescence (CPL) dissymmetry, quantified by the g_{CPL} values, accompanied by a high photoluminescence quantum yield (PLQY, Φ). In this context, numerous chiral organic molecules have been investigated[3] ranging from thermally activated delayed fluorescence (TADF) materials[4] to aggregation-induced emission (AIE) materials.[5] Furthermore, investigation has extended to metal complexes incorporating Ir (III),[6] Pt(II)[7] ions, as well as lanthanoids,[8] all coordinated by chiral ligands, owing to their considerable spin–orbit coupling, which results in phosphorescence from the triplet excited states. We have also reported that Pt(II) complexes coordinated by a prevalent chiral ligand, 2,2′-binaphthol (BINOL), exhibited aggregation-induced circularly polarized phosphorescence.[7q] However, the acquired PLQY was exceedingly low, and the g-values were in the moderate magnitude, compared with analogous chiral Pt(II) complexes.

Chiral Zn(II) complexes, recognized for their relatively economical cost and low toxicity, have been reported to exhibit CPL.[9] For example, a dipyrromethene-based chiral Zn(II) complex has been elucidated by Hasobe *et al.* to demonstrate a noteworthy PLQY of $\Phi = 23\%$ and a high g-value of $g_{CPL} = \pm0.022$.[9f] CP-OLEDs employing a Zn(II) complex with chiral salen-type ligands as a CPL emitter have been fabricated by Tang *et al.* exhibiting substantial g_{EL} values of ±0.044, as well as external quantum efficiencies (EQE) of 0.038% for the *R*-enantiomer and 0.042% for the *S*-enantiomer, respectively.[9g] In this context, we focused on Zn(II) complexes coordinated by chiral Schiff-base type ligands derived from the commercially available BINOL, motivated by the prolific nature of metal complexes featuring Schiff-base type ligands known for their

[a]Graduate School of Science and Engineering, Ibaraki University, 2-1-1 Bunkyo, Mito, Ibaraki 310-8512, Japan. E-mail: hiroyuki.nishikawa.sci@vc.ibaraki.ac.jp
[b]Graduate School of Science, Kitasato University, Kanagawa 252-0373, Japan
[c]Graduate School of Life and Environmental Sciences, Kyoto Prefectural University, Kyoto 606-8522, Japan
[d]Graduate School of Science, Tokyo Metropolitan University, Tokyo, 192-0397, Japan
[e]Faculty of Pure and Applied Sciences, University of Tsukuba, Tsukuba 305-8577, Japan

†Electronic supplementary information (ESI) available: Crystallographic data, spectroscopic data and results of theoretical calculation. CCDC 2340521 for **R-Zn** and 2340522 for **S-Zn**. For ESI and crystallographic data in CIF or other electronic format see DOI: https://doi.org/10.1039/d4dt00903g
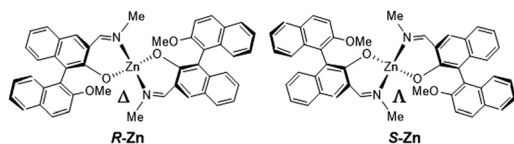
Fig. 1 Molecular structure of *R*/*S*-Zn.

remarkable PLQY.[10] A pair of novel chiral Zn(ɪɪ) complexes co-ordinated with the Schiff-base type BINOL ligands (*R*-Zn and *S*-Zn, Fig. 1) were synthesized, exhibiting aggregation-induced enhanced emission (AIEE) characteristics along with a high photoluminescence. We elucidated the structures of both enantiomers by X-ray structural analyses, concurrently probing their chiroptical properties through spectroscopic measurements. In both the solution and solid states, the *R*-Zn and *S*-Zn exhibited circular dichroism (CD) and CPL spectra with *g*-values of comparable magnitudes to those for previously reported chiral Zn(ɪɪ) complexes. Interestingly, a reversal in the sign of CPL signals has been observed between the solution and solid states. Furthermore, the employment of density functional theory (DFT) molecular orbital computations has imparted theoretical elucidation, regarding the detailed electronic structures of enantiomers, including the simulation of their CD spectra.

Results and discussion

Synthesis

The Schiff-base type chiral ligands derived from BINOL were synthesized according to the previous reports.[11] *R*-/*S*-Zn were synthesized by the reaction of the chiral binaphthyl precursor *R*-/*S*-1 with zinc acetate in the presence of methyl amine, yielding a lemon-yellow powder (Scheme 1).

X-ray structural analyses

X-ray crystal structure analyses of *R*-Zn and *S*-Zn were performed at 100 K for the plate-shaped single crystals recrystallized from CH_2Cl_2/MeOH. Crystallographic data are listed in Table S1.† Both enantiomers crystalized in the monoclinic, non-centrosymmetric space group *C*2. Fig. 2 shows the molecular and crystal structures of *R*-Zn. The configuration of *S*-Zn was a complete mirror image of its *R*-enantiomer. The asymmetric unit comprises two crystallographically independent complex molecules and a disordered water molecule, wherein
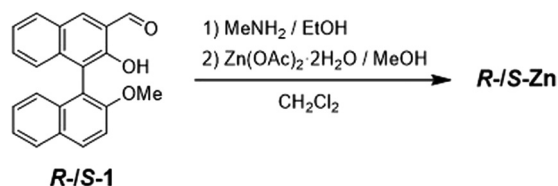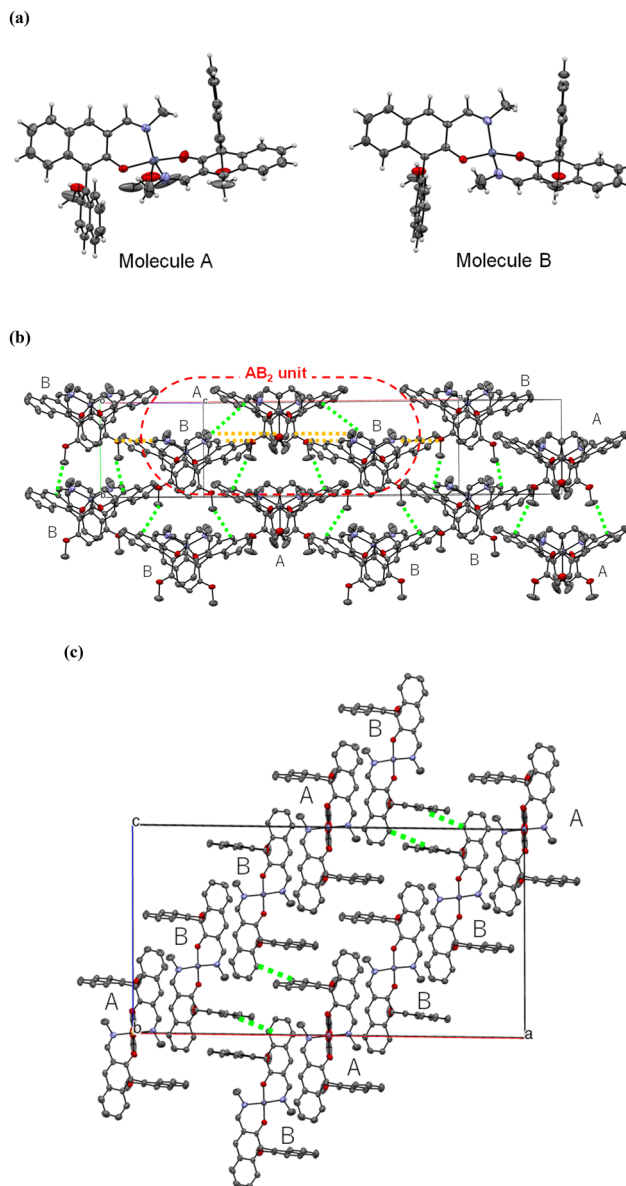

Fig. 2 Crystal structure of *R*-Zn. (a) Molecular structure of *R*-Zn; molecule A (left) and molecule B (right); (b) crystal structure of *R*-Zn (green dotted line: CH···π interactions, orange dotted line: CH···O interactions); (c) crystal structure of *R*-Zn projected along *b*-axis.

one corresponds to half of the complex identified as molecule A, and the other represents the complex identified as molecule B (Fig. 2a). The Zn(ɪɪ) ion within molecule A is additionally co-ordinated by a methanol molecule, adopting a distorted trigonal–bipyramidal geometry. The bond angles around Zn(ɪɪ) ion are 90.57(11)°–96.75(12)° (O–Zn–N) and 164.5(2) (O–Zn–O). A 2-fold rotational axis exists along the axis passing through the Zn(ɪɪ) ion and the oxygen atom of coordinated methanol, inducing the positional disorder in the methyl group of the methanol. Contrarily, the Zn(ɪɪ) ion within molecule B assumes a distorted tetrahedral configuration (95.88(11)°–106.95 (N–Zn–O) and 130.28(11) (O–Zn–O)) in the absence of methanol coordi-

1) MeNH₂ / EtOH
2) Zn(OAc)₂·2H₂O / MeOH
   CH_2Cl_2
→ *R*-/*S*-Zn

R-/*S*-1

Scheme 1 .

nation. The coordination bond length around the Zn(II) ions lie in the range of 1.996(3)–2.061(3) Å for Zn–N and 1.906(2)–1.960(2) Å for Zn–O, representing values typical of Schiff-base type Zn(II) complexes.[9d,e,10a,c,d,g] The dihedral angles between the two naphthyl groups within **R-Zn** are 88° and 90°, slightly larger than those for Pt(II) complexes coordinated by the Schiff-base type binaphthyl ligands and BINOL ligands.[7p,q] In general, metal complexes featuring tetrahedral and trigonal–bipyramidal geometries coordinated by two asymmetrical bidentate ligands exhibit enantiomeric isomers at the metal center (Λ- and Δ-configuration). In the present Zn(II) complexes, notably, either diastereomer was selectively obtained. Specifically, the chiral ligands **R-1** and **S-1** lead to Δ-**R-Zn** and Λ-**S-Zn**, respectively, probably due to the steric hindrance imposed by the chiral BINOL ligands. Similar diastereoselectivity has been reported for dissymmetric tetrahedral metal complexes employing chiral Schiff-base type ligands.[12]

The symmetry operation by the 2-fold rotational axis inherent in molecule A gives rise to three complexes, composed of one molecule A and two molecules B as shown in Fig. 2b. In this AB_2 unit, several CH···π intermolecular interactions are present between molecule A and B (2.867 Å: between the naphthyl carbon of molecule A and the naphthyl hydrogen of molecule B, 2.900 Å: between the naphthyl carbon of molecule A and the hydrogen of methyl group located on the imine nitrogen of molecule B), along with CH···O interactions (2.547 Å: between the methoxy oxygen of molecule A and the hydrogen located on the imine carbon of molecule B, 2.523 Å: between the methoxo oxygen in coordinated methanol of molecule A and the naphthyl hydrogen of molecule B). Additionally, between the AB_2 units, an intermolecular CH···O interaction exists between the hydrogen located on the imine carbon of molecule B and the methoxy oxygen of the adjacent molecule B with a distance of 2.581 Å (Fig. 2b), leading to the 1-dimensional chain along the (1/2, 1/2, 1) direction (Fig. 2c). Furthermore, intermolecular interactions through CH···π contacts exist between 1-dimensional chains both along *a*- and *b*-axis. Consequently, 3-dimensional intermolecular interactions induce a rigid crystal that constrains the vibrational motions of the molecules, thereby resulting in AIEE characteristics (*vide infra*).

Photophysical properties

The UV-vis absorption spectra of **R-Zn** and **S-Zn** were acquired for CH_2Cl_2 solutions at a concentration of 10^{-5} M and powder samples dispersed in KBr pellets with a concentration of 0.1 wt% (Fig. 3a and Fig S8, 9†). The similar characteristics in the observed absorption spectra between solutions and solid states indicate the absence of intermolecular electronic interaction in the solid states despite numerous CH···π and CH···O contacts between complexes. The absorption spectra were calculated using the time-dependent density functional theory (TD-DFT) method at the level of CAM-B3LYP/Def2-SVP for **R-Zn** in the absence of MeOH coordination (Fig. 2a). The initial geometry was derived from the molecular structure of molecule B determined by the X-ray crystallography, subsequently opti-
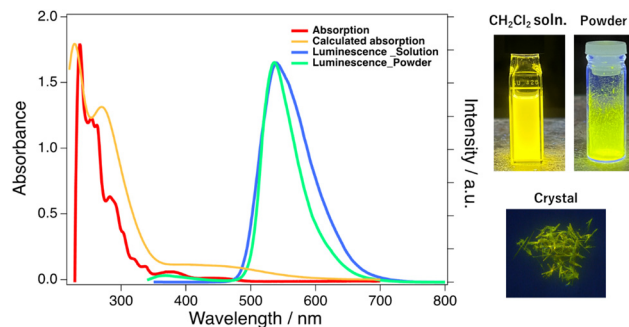

Fig. 3 (a) Absorption spectrum of **R-Zn** (red, 1.0×10^{-5} M in CH_2Cl_2), the calculated spectrum (orange), and emission spectra in 1.0×10^{-4} M CH_2Cl_2 solution (blue) and in powder (green) excited at 300 nm; (b) photographs of emission of **R-Zn** in a CH_2Cl_2 solution (upper left), in powder (upper right) and in crystals (lower).

mized through the density functional theory (DFT) incorporating the conductor-like polarizable continuum model (CPCM) to consider the solvent (CH_2Cl_2). The optimized molecular structures and their coordinates are summarized in Fig. S16 and Table S4.† The selected TD-DFT calculated excitation energies corresponding to the experimental absorption wavelengths, and related molecular orbitals (MOs) are summarized in Table S3 and Fig. S15.† The dominant transition at the absorption edge (~473 nm) is associated with the transition from the highest occupied MO (HOMO) to the lowest unoccupied MO (LUMO), corresponding to the ligand-centered π–π* (binaphthyl moieties) local excitations. The small absorption band, exhibiting a peak at 379 nm, can similarly be assigned to the ligand-centered π–π* (binaphthyl moieties) excitations. The higher energy absorption bands observed at 282 nm can be assigned to the inter-ligand charge transfer (LL'CT) band, while the absorption bands observed at 236 nm can be assigned to the mixture of the ligand-centered π–π* (binaphthyl moieties) excitations and the LL'CT band. These results calculated by TD-DFT methods suggest that most electronic transition processes of **R-Zn** are mainly attributed to the intra-ligand π–π* local excitation and LL'CT, with quite a little contribution from the 3d orbital of the Zn(II) ion, similar to previously reported luminescent Zn(II) complexes.[9c–e,10b,g]

The emission spectra of **R-Zn** and **S-Zn** were measured for CH_2Cl_2 solution (10^{-4} M) and powder samples, displaying in Fig. 3a (blue line: solution and green line: powder), along with photographs of luminescent samples (Fig. 3b). The fluorescence spectrum of a CH_2Cl_2 solution of **R-Zn** exhibited a broad yellow emission, characterized by a peak wavelength centered at 536 nm. Similarly, the powder sample exhibited an emission with a peak at 536 nm, but a reduction in bandwidth compared to the solution was observed, resulting in a greenish-yellow emission (Fig. 3b). The photoluminescence quantum yields (PLQYs) in CH_2Cl_2 solutions were 12% for both enantiomers, closely resembling the values reported for chiral Zn(II) complexes previously.[9c,d,f,g,10a,c,f,h] In contrast, the PLQYs of the powder (**R-Zn**: 26%; **S-Zn**: 25%) exhibited twofold

enhancement compared to those in CH_2Cl_2 solutions, indicating the aggregation-induced enhanced emission (AIEE) property. The AIEE is ascribed to restraint of the molecular motion within the solid state, induced by 3-dimensional intermolecular interactions as revealed by X-ray crystallography. The photoluminescence decay curves of both the solution and powder samples were fitted by a single exponential function (Fig. S10 and 11†), yielding comparable lifetimes for both the solution and powder samples (**R-Zn**: 8.7 ns (solution), 8.7 ns (powder); **S-Zn**: 8.7 ns (solution), 9.1 ns (powder)), suggesting fluorescence consistent with previous reports.[9a,b,d,f]

Chiroptical properties

The chiroptical properties of **R-/S-Zn** both in solution and solid states were elucidated by CD and CPL spectroscopies. CD spectra were acquired for CH_2Cl_2 solutions (1.0×10^{-5} M) and powder samples dispersed in KBr (0.1 wt%). As shown in Fig. 4a, clear mirror image CD spectra were observed with prominent Cotton effects between 230 and 300 nm, corresponding to local excitation in the BINOL ligand. The estimated g_{abs} values of **R-/S-Zn** were similar to be 2.0×10^{-3} at 265 nm, exhibiting a comparable magnitude to those obtained for previously reported chiral Zn(II) complexes.[9a] The CD spectra ranging from 230 to 500 nm were well reproduced by TD-DFT calculations for the molecule B (Fig. 4b). The electric transitions correspond to intra-ligand excitation and LL'CT in accordance with the absorption spectra (Fig. S14†). In contrast, the CD spectra obtained for KBr pellets exhibited distinct difference compared to those observed for CH_2Cl_2 solutions (Fig. 4a); ellipticity at longer wavelengths (300–500 nm) surpassed that at shorter wavelengths (<300 nm). The divergence in the CD spectra can be attributed to the distinct configuration present in the solid state, specifically structural deformation induced by intermolecular CH···π and CH···O interaction, and/or existence of two complexes exhibiting different coordination geometries, namely a trigonal–bipyramidal structure with a 5-coordination site and a distorted tetrahedral coordination.

The CPL spectra were acquired for CH_2Cl_2 solutions (1.0×10^{-4} M) and powder samples. As shown in Fig. 5a and b, both the CPL signals of **R-/S-Zn** in CH_2Cl_2 solutions and powders

Fig. 5 (a) CPL spectra (upper) and emission spectra (lower) of **R-Zn** (red) and **S-Zn** (blue) in CH_2Cl_2 (1.0×10^{-4} M) excited at 300 nm; (b) CPL spectra (upper) and emission spectra (lower) of **R-Zn** (red) and **S-Zn** (blue) in powder states excited at 300 nm.

exhibited mirror images. The CH_2Cl_2 solutions displayed broad signals at 524 nm with g_{CPL} values of 0.86×10^{-3} (**R-Zn**) and -0.84×10^{-3} (**S-Zn**), respectively. Contrarily, the powders exhibited sigmoidal signals and a reversal of the sign of the CPL signals at 541 nm compared to the signals observed in solutions; the g_{CPL} values were estimated to be -0.62×10^{-3} (**R-Zn**) and 1.0×10^{-3} (**S-Zn**), respectively. These g_{CPL} values are in the same order of magnitude to the previously reported chiral Zn(II) complexes.[9a,b,d,e] The reversal of the sign of CPL signals has been reported in various BINOL-based materials, depending on the dihedral angles between two naphthyl groups.[13] Consequently, intermolecular interactions in the solid state probably induced alterations in the dihedral angles of **R-/S-Zn** from those in solutions; the dihedral angles between the two naphthyl groups within the optimized **R-/S-Zn** structures are notably small (69° and 72°) in contrast to those determined by X-ray diffraction on single crystals. This difference in the dihedral angles may result in the observed sign reversal. An alternative interpretation for the inversion of sign may be attributed to the coexistence of two types of complexes characterized by different coordination geometries existing in the crystals.

Conclusions

Novel chiral Zn(II) complexes exhibiting AIEE properties, **R-/S-Zn**, were synthesized using a chiral BINOL ligand featuring a Schiff-base type coordination site. X-ray crystallography revealed the presence of two crystallographically independent complexes within the single crystal: a trigonal–bipyramidal complex coordinated with two binaphthyl ligands and MeOH (molecule A), and a distorted tetrahedral complex coordinated with two binaphthyl ligands (molecule B). Intermolecular interactions through CH···π and CH···O contacts result in a 1-dimensional chain composed of AB_2 units. Between 1-dimensinal chains, intermolecular CH···π interactions exist, leading to the formation of a 3-dimensional rigid network structure. Fluorescence was observed in both CH_2Cl_2 solutions and powder samples. The PLQYs of the powders were twice as
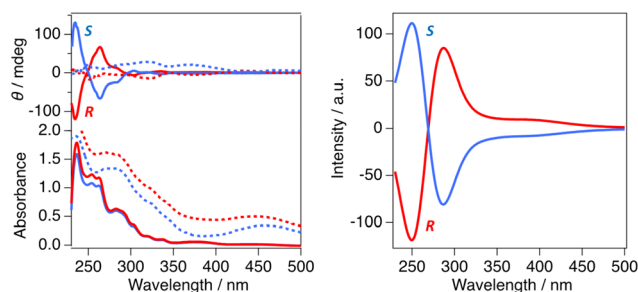

Fig. 4 (a) CD spectra (upper) and absorption spectra (lower) of **R-Zn** and **S-Zn** in 1.0×10^{-5} M CH_2Cl_2 (**R-Zn**: red solid line, **S-Zn**: blue solid line) and in 0.1 wt% KBr pellet (**R-Zn**: red dotted line, **S-Zn**: blue dotted line); (b) calculated CD spectra of **R-Zn** (red) and **S-Zn** (blue).
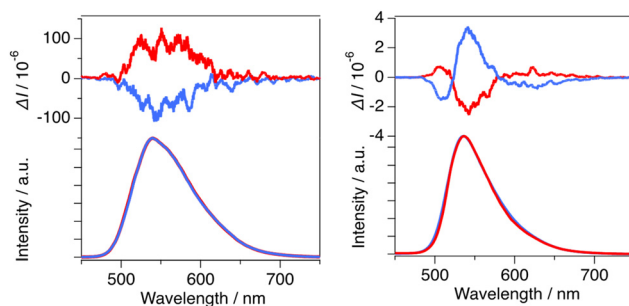
large as those of solutions, thereby affirming the presence of AIEE properties. The intense emission from the aggregates can be attributed to the restraint of the molecular motion induced by 3-dimensional intermolecular interactions. Both the CD and CPL spectra were observed for both solution and powder samples. However, the spectral characteristics exhibited significant disparities between the solutions and powders, probably owing to the deformation of the molecular structures induced by the intermolecular interaction, and/or the coexistence of two types of complexes with different coordination geometries in the solid states. The dissymmetry factors were comparable to those of analogous chiral Zn(ɪɪ) complexes reported previously. While the *g*-values of **R-**/**S-Zn** were not remarkable, we have achieved notable emission from the solid states with pronounced AIEE properties. The findings from this study offer valuable insights not only for the development of CP-OLED but also for diverse fields regarding the chiroptics.

Experimental section

Synthesis and methods

All reagents and solvents were of the commercial reagent grade and used without further purification unless otherwise noted. CH_2Cl_2 was distilled from CaH_2. All the compounds were identified by ^{1}H-NMR (Fig. S1 and S2†), ^{13}C-NMR (Fig. S3 and S4†), elemental analysis, and ESI-MS. The assignment of individual protons was further conducted by 2D-NMR measurements, including COSY and NOESY spectroscopy (Fig. S5 and S6†). ^{1}H-and ^{13}C-NMR spectra were recorded on a BRUKER AVANCE III 500 at 25 °C in d_6-DMSO or *d*-chloroform. ^{1}H-NMR chemical shifts are expressed in parts per million (δ) relative to trimethyl silane (TMS) as a reference. Mass spectra were obtained with a JEOL MStation JMS-700.

General procedure for synthesis of **R-Zn** and **S-Zn**

The synthesis of **R-Zn** is representative. A mixture of (*R*)-2-hydroxy-2′-methoxy-[1,1′-binaphthalene]-3-carbaldehyde (**1**) (107 mg, 0.327 mmol) and 9% MeNH$_2$/EtOH solution (50 μL) in CH_2Cl_2 was stirred for 30 minutes at room temperature. After removal of the solvent and excess MeNH$_2$ under vacuum, the residue was dissolved in CH_2Cl_2. To CH_2Cl_2 solution was added MeOH solution of Zn(OAc)$_2$·2H$_2$O (46.2 mg, 0.210 mmol), and the reaction mixture was stirred overnight leading to a color change from pale yellow to yellow. The solvent was evaporated *in vacuo*, and the residue was washed with MeOH and recrystallized from CH_2Cl_2/MeOH to give **R-Zn** as lemon-yellow crystals in 15% yield (37 mg, 0.0496 mmol).

(*R*)-[ZnL$_2$] (**R-Zn**): ^{1}H-NMR (500 MHz, d_6-DMSO): δ2.55 (s, 3H), 3.65 (s, 3H), 6.63 (d, *J* = 8.5 Hz, 1H), 6.96 (t, *J* = 7.3 Hz, 1H), 7.02–7.06 (m, 2H), 7.10 (t, *J* = 7.5 Hz, 1H), 7.26 (t, *J* = 7.5 Hz, 1H), 7.52 (d, *J* = 9.0 Hz, 1H), 7.69 (d, *J* = 8.0 Hz, 1H), 7.82 (s, 1H), 7.88 (d, *J* = 8.0 Hz, 1H), 7.96 (d, *J* = 9.0 Hz, 1H), and 8.31 (s, 1H) ppm; ^{13}C-NMR (500 MHz, *d*-CHCl$_3$): δ166.3, 154.9, 135.3, 133.9, 132.6, 129.6, 129.4, 128.7, 128.0, 127.9, 127.3, 126.4, 125.1, 124.9, 123.6, 123.1, 121.0, 119.0, 117.3, 114.3,

57.0, 46.3 ppm; ESI-MS: *m/z* 745.2016 (M + H$^+$); Anal. Calcd for C$_{46}$H$_{36}$N$_2$O$_4$Zn·1.5H$_2$O: C 71.59, H 4.90, N 3.63. Found: C 71.60, H 4.93, N 3.59.

(*S*)-[ZnL$_2$] (**S-Zn**): ^{1}H-NMR (500 MHz, d_6-DMSO): δ2.55 (s, 3H), 3.65 (s, 3H), 6.63 (d, *J* = 8.5 Hz 1H), 6.96 (t, *J* = 7.3 Hz, 1H), 7.02–7.06 (m, 2H), 7.10 (t, *J* = 7.5 Hz, 1H), 7.26 (t, *J* = 7.3 Hz, 1H), 7.52 (d, *J* = 9.0 Hz, 1H), 7.69 (d, *J* = 8.0 Hz, 1H), 7.82 (s, 1H), 7.88 (d, *J* = 8.5 Hz, 1H), 7.96 (d, *J* = 9.0 Hz, 1H), and 8.31 (s, 1H) ppm; ^{13}C-NMR (500 MHz, *d*-CHCl$_3$): δ166.2, 154.8, 135.2, 133.8, 132.6, 129.6, 129.3, 128.7, 128.0, 127.9, 127.3, 126.5, 125.0, 124.8, 123.5, 123.1, 120.9, 118.8, 117.2, 114.1, 56.9, 46.3 ppm; ESI-MS: *m/z* 745.2593 (M + H$^+$); Anal. Calcd for C$_{46}$H$_{36}$N$_2$O$_4$Zn·2.5H$_2$O: C 69.82, H 5.20, N 3.54. Found: C 69.53, H 4.80, N 3.40.

X-ray crystallography

A single crystal of **R-Zn** or **S-Zn** was mounted on a roop with paraton oil. Diffraction data were collected at 100 K on a Rigaku XtaLAB P200 diffractometer fitted with a CCD-type area detector, and a full sphere of data was collected using graphite-monochromated Mo Kα radiation (λ = 0.71073 Å). Data frames were integrated with the CrysAlisPro software and merged to give a unique data set for structure analysis. The structures were solved by direct methods and refined by the full-matrix least-squares method on F^2 data with the SHELXL-2016/6 package. All non-hydrogen atoms were refined with anisotropic thermal parameters. Hydrogen atoms were included in calculated positions and refined with isotropic thermal parameters riding on those of the parent atoms. Crystallographic data and structure refinement details are listed in Table S1.†

Spectroscopy

UV-vis absorption spectra of CH_2Cl_2 solutions (1.0×10^{-5} M) and 0.1 wt% KBr pellets were recorded with JASCO V-570 UV/VIS/NIR spectrometer. CD spectra of CH_2Cl_2 solutions (1.0×10^{-5} M) and 0.1 wt% KBr pellets were recorded with JASCO J-720 W spectrometer. KBr pellets for the measurements of UV-vis absorption and CD spectra were prepared by mixing KBr and samples and compressing at 40 MPa for 5 minutes. Powder samples in the solid state for the other spectroscopic measurements (photoluminescence, CPL and fluorescence lifetime) were prepared by dropping the MeOH suspension of the Zn complex onto the glass substrate, followed by spontaneous evaporation of the MeOH solvent. Photoluminescence spectra of CH_2Cl_2 solutions (1.0×10^{-4} M) and the solid state (powder samples) were acquired using JASCO FP-8600 spectrometer at room temperature, at excitation wavelength of 300 nm (both solutions and powders). CPL spectra of CH_2Cl_2 solutions (1.0×10^{-4} M) and powder samples were measured with a JASCO CPL-300 spectrofluoropolarimeter at room temperature, at a scattering angle of 0° upon excitation with unpolarized, monochromated incident light with a 20 nm bandwidth for solutions and 25 nm bandwidth for the powder samples. Absolute PLQYs of solutions and powder samples were determined using a JASCO PF-6500 spectrometer with an integrat-

ing sphere (JASCO ILF-533, diameter 96 mm) at excitation wavelength of 300 nm. The preparation of quantum yield measurement samples for powders involved the utilization of KBr plates, between which powders were interposed, under the application of a pressure of 20 MPa. Fluorescence lifetimes were measured for solutions and powder samples with a HORIBA DeltaFlex spectrometer with a 370 nm LED light source for excitation. For the lifetime measurements of solutions, a conventional 1 cm quartz cell was used.

DFT calculations

All calculations were performed by using Gaussian 16 rev C.02 program package.[14] The initial geometry was taken from the X-ray crystal structure analysis and optimized by the density functional theory (DFT) at the level of CAM-B3LYP[15]/Def2-SVP for all atoms with the conductor-like polarizable continuum model (CPCM)[16] to consider the solvent (CH_2Cl_2). The Optimized equilibrium structures were confirmed by normal coordinate analyses, with no imaginary frequency found (Tables S4 and S5†). The time-dependent density functional theory (TD-DFT)[17] calculation for *R*-Zn was conducted at the level of CAM-B3LYP/Def-2SVP for all atoms with the conductor-like polarizable continuum model (CPCM) to consider the solvent (CH_2Cl_2). The UV-vis absorption spectrum of *R*-Zn was simulated based on the 100 of the calculated oscillation strengths with Gaussian distribution. The CD spectrum of *R*-Zn and *S*-Zn were also simulated based on 100 of the calculated rotatory strengths (Fig. S14†). Representative calculated singlet vertical excitation energies with relatively large oscillation strengths and rotatory strengths in CH_2Cl_2 are summarized in Table S3† and corresponding molecular orbitals are depicted in Fig. S15.†

Conflicts of interest

There are no conflicts to declare.

Acknowledgements

References

1 (*a*) B. Kunnen, C. Macdonald, A. Doronin, S. Jacques, M. Eccles and I. Meglinski, *J. Biophotonics*, 2015, **8**, 317–323; (*b*) L. E. MacKenzie and R. Pal, *Nat. Rev. Chem.*, 2021, **5**, 109–124; (*c*) J. Gong and X. Zhang, *Coord. Chem. Rev.*, 2022, **453**, 214329; (*d*) J. F. Sherson, H. Krauter, R. K. Olsson, B. Julsgaard, K. Hammerer, I. Cirac and E. S. Polzik, *Nature*, 2006, **443**, 557–560; (*e*) D. W. Zhang, M. Li and C. F. Chen, *Chem. Soc. Rev.*, 2020, **49**, 1331–1343.

2 (*a*) D.-Y. Kim, *J. Korean Chem. Soc.*, 2006, **49**, S505–S508; (*b*) C. Li, X. Yang, J. Han, W. Sun and P. Duan, *Mater. Adv.*, 2021, **2**, 3851–3855; (*c*) H. Li, H. Li, W. Wang, Y. Tao, S. Wang, Q. Yang, Y. Jiang, C. Zheng, W. Huang and R. Chen, *Angew. Chem., Int. Ed.*, 2020, **59**, 4756–4762; (*d*) N. Nishizawa, B. Al-Qadi and T. Kuchimaru, *J. Biophotonics*, 2021, **14**, e202000380.

3 (*a*) L. Arrico, L. Di Bari and F. Zinna, *Chem. – Eur. J.*, 2021, **27**, 2920–2934; (*b*) F. Pop, N. Zigon and N. Avarvari, *Chem. Rev.*, 2019, **119**, 8435–8478.

4 (*a*) Z.-P. Yan, T.-T. Liu, R. Wu, X. Liang, Z.-Q. Li, L. Zhou, Y.-X. Zheng and J.-L. Zuo, *Adv. Funct. Mater.*, 2021, **31**, 2103875; (*b*) F.-M. Xie, J.-X. Zhou, X.-Y. Zeng, Z.-D. An, Y.-Q. Li, D.-X. Han, P.-F. Duan, Z.-G. Wu, Y.-X. Zheng and J.-X. Tang, *Adv. Opt. Mater.*, 2021, **9**, 2100017; (*c*) L. Frédéric, A. Desmarchelier, L. Favereau and G. Pieters, *Adv. Funct. Mater.*, 2021, **31**, 2010281; (*d*) Y. Yang, N. Li, J. Miao, X. Cao, A. Ying, K. Pan, X. Lv, F. Ni, Z. Huang, S. Gong and C. Yang, *Angew. Chem., Int. Ed.*, 2022, **61**, e202202227; (*e*) T. Hua, J. Miao, H. Xia, Z. Huang, X. Cao, N. Li and C. Yang, *Adv. Funct. Mater.*, 2022, **32**, 2201032.

5 (*a*) A. Nitti and D. Pasini, *Adv. Mater.*, 2020, **32**, 1908021; (*b*) J. Hwang, P. Nagaraju, M. J. Cho and D. H. Choi, *Aggregate*, 2022, e199; (*c*) N. Masimukku, D. Gudeika, D. Volyniuk, O. Bezvikonnyi, J. Simokaitiene, V. Matulis, D. Lyakhov, V. Azovskyi and J. V. Gražulevičius, *Phys. Chem. Chem. Phys.*, 2022, **24**, 5070–5082; (*d*) C. Liu, J.-C. Yang, J. W. Y. Lam, H.-T. Feng and B. Z. Tang, *Chem. Sci.*, 2022, **13**, 611–632; (*e*) J. Roose, B. Z. Tang and K. S. Wong, *Small*, 2016, **12**, 6495–6512; (*f*) Z. Geng, Z. Liu, H. Li, Y. Zhang, W. Zheng, Y. Quan and Y. Cheng, *Adv. Mater.*, 2022, **35**, 2209495; (*g*) L. Yang, Y. Zhang, X. Zhang, N. Li, Y. Quan and Y. Cheng, *Chem. Commun.*, 2018, **54**, 9663–9666; (*h*) R. Hu, Y. Yuan, M. Gu and Y.-Q. Zou, *Eng. Regen.*, 2022, **3**, 323–338; (*i*) H.-T. Feng, C. Liu, Q. Li, H. Zhang, J. W. Y. Lam and B. Z. Tang, *ACS Mater. Lett.*, 2019, **1**, 192–202; (*j*) M. M. Talamo, T. Cauchy, F. Pop, F. Zinna, L. Di Bari and N. Avarvari, *J. Mater. Chem. C*, 2023, **11**, 5701–5713.

6 (*a*) T.-Y. Li, Y.-M. Jing, X. Liu, Y. Zhao, L. Shi, Z. Tang, Y.-X. Zheng and J.-L. Zuo, *Sci. Rep.*, 2015, **5**, 14912; (*b*) J. Han, S. Guo, J. Wang, L. Wei, Y. Zhuang, S. Liu, Q. Zhao, X. Zhang and W. Huang, *Adv. Opt. Mater.*, 2017, **5**, 1700359; (*c*) T.-Y. Li, Y.-X. Zheng and Y.-H. Zhou, *Dalton Trans.*, 2016, **45**, 19234–19237; (*d*) Y. Wang, T. Harada, Y. Shiota, K. Yoshizawa, H. Wang, S. Wang, X. Ye, M. Ogasawara and T. Nakano, *RSC Adv.*, 2017, **7**, 29550–29553; (*e*) J.-J. Lu, Z.-L. Tu, X.-F. Luo, Y.-P. Zhang, Z.-Z. Qu,

X. Liang, Z.-G. Wu and Y.-X. Zheng, *J. Mater. Chem. C*, 2021, **9**, 5244–5249; (*f*) M. Ashizawa, L. Yang, K. Kobayashi, H. Sato, A. Yamagishi, F. Okuda, T. Harada, R. Kuroda and M.-a. Haga, *Dalton Trans.*, 2009, 1700–1702; (*g*) G. Cheng, J.-J. Lu, L.-Y. Zhu and G. Lu, *Micro Nano Lett.*, 2023, **18**, e12169; (*h*) Z.-P. Yan, K. Liao, H.-B. Han, J. Su, Y.-X. Zheng and J.-L. Zuo, *Chem. Commun.*, 2019, **55**, 8215–8218.

7 (*a*) B. Yang, G. Zou, S. Zhang, H. Ni, H. Wang, W. Xu, C. Yang, H. Zhang, W. Yu and K. Luo, *Angew. Chem., Int. Ed.*, 2021, **60**, 10531–10536; (*b*) G. Qian, X. Yang, X. Wang, J. D. Herod, D. W. Bruce, S. Wang, W. Zhu, P. Duan and Y. Wang, *Adv. Opt. Mater.*, 2020, **8**, 2000775; (*c*) S. G. Kang, K. Y. Kim, Y. Cho, D. Y. Jeong, J. H. Lee, T. Nishimura, S. S. Lee, S. K. Kwak, Y. You and J. H. Jung, *Angew. Chem., Int. Ed.*, 2022, **61**, e202207310; (*d*) J. R. Brandt, X. Wang, Y. Yang, A. J. Campbell and M. J. Fuchter, *J. Am. Chem. Soc.*, 2016, **138**, 9743–9746; (*e*) Z.-P. Yan, X.-F. Luo, W.-Q. Liu, Z.-G. Wu, X. Liang, K. Liao, Y. Wang, Y.-X. Zheng, L. Zhou, J.-L. Zuo, Y. Pan and H. Zhang, *Chem. – Eur. J.*, 2019, **25**, 5672–5676; (*f*) B. Yang, H. Ni, H. Wang, Y. Hu, K. Luo and W. Yu, *J. Phys. Chem. C*, 2020, **124**, 23879–23887; (*g*) M. Ikeshita, S. Furukawa, T. Ishikawa, K. Matsudaira, Y. Imai and T. Tsuno, *ChemistryOpen*, 2022, **11**, e202100277; (*h*) H. Zhu, Q. Li, B. Shi, H. Xing, Y. Sun, S. Lu, L. Shangguan, X. Li, F. Huang and P. J. Stang, *J. Am. Chem. Soc.*, 2020, **142**, 17340–17345; (*i*) Y.-P. Zhang and Y.-X. Zheng, *Dalton Trans.*, 2022, **51**, 9966–9970; (*j*) Z.-L. Gong and Y.-W. Zhong, *Sci. China: Chem.*, 2021, **64**, 788–799; (*k*) J. Song, H. Xiao, L. Fang, L. Qu, X. Zhou, Z.-X. Xu, C. Yang and H. Xiang, *J. Am. Chem. Soc.*, 2022, **144**, 2233–2244; (*l*) L. Yuan, Q.-J. Ding, Z.-L. Tu, X.-J. Liao, X.-F. Luo, Z.-P. Yan, Z.-G. Wu and Y.-X. Zheng, *Chin. Chem. Lett.*, 2022, **33**, 1459–1462; (*m*) B. Li, Y. Li, M. H. Chan and V. W. Yam, *J. Am. Chem. Soc.*, 2021, **143**, 21676–21684; (*n*) X.-P. Zhang, V. Y. Chang, J. Liu, X.-L. Yang, W. Huang, Y. Li, C.-H. Li, G. Muller and X.-Z. You, *Inorg. Chem.*, 2015, **54**, 143–152; (*o*) T. Biet, T. Cauchy, Q. Sun, J. Ding, A. Hauser, P. Oulevey, T. Burgi, D. Jacquemin, N. Vanthuyne, J. Crassous and N. Avarvari, *Chem. Commun.*, 2017, **53**, 9210–9213; (*p*) J. Song, M. Wang, X. Zhou and H. Xiang, *Chem. – Eur. J.*, 2018, **24**, 7128–7132; (*q*) D. Tauchi, T. Koida, Y. Nojima, M. Hasegawa, Y. Mazaki, A. Inagaki, K. I. Sugiura, Y. Nagaya, K. Tsubaki, T. Shiga, Y. Nagata and H. Nishikawa, *Chem. Commun.*, 2023, **59**, 4004–4007.

8 (*a*) Y. Zhong, Z. Wu, Y. Zhang, B. Dong and X. Bai, *InfoMat*, 2022, **5**, e12392; (*b*) M. Starck, L. E. MacKenzie, A. S. Batsanov, D. Parker and R. Pal, *Chem. Commun.*, 2019, **55**, 14115–14118; (*c*) M. Deng, N. D. Schley and G. Ung, *Chem. Commun.*, 2020, **56**, 14813–14816; (*d*) F. Zinna, U. Giovanella and L. Di Bari, *Adv. Mater.*, 2015, **27**, 1791–1795; (*e*) F. Zinna and L. Di Bari, *Chirality*, 2015, **27**, 1–13; (*f*) Y. B. Tan, Y. Okayasu, S. Katao, Y. Nishikawa, F. Asanoma, M. Yamada, J. Yuasa and T. Kawai, *J. Am. Chem. Soc*, 2020, **142**, 17653–17661; (*g*) A. Abhervé, M. M. Talamo, N. Vanthuyne, F. Zinna, L. Di Bari,

M. Grasser, B. Le Guennic and N. Avarvari, *Eur. J. Inorg. Chem.*, 2022, **2022**, e202200010.

9 (*a*) Y. Wang, X. Li, L. Yang, W.-Y. Sun, C. Zhu and Y. Cheng, *Mater. Chem. Front.*, 2018, **2**, 554–558; (*b*) J. F. Kögel, S. Kusaka, R. Sakamoto, T. Iwashima, M. Tsuchiya, R. Toyoda, R. Matsuoka, T. Tsukamoto, J. Yuasa, Y. Kitagawa, T. Kawai and H. Nishihara, *Angew. Chem., Int. Ed.*, 2015, **55**, 1377–1381; (*c*) Y. Tanaka, T. Murayama, A. Muranaka, E. Imai and M. Uchiyama, *Chem. – Eur. J.*, 2020, **26**, 1768–1771; (*d*) M. Savchuk, S. Vertueux, T. Cauchy, M. Loumaigne, F. Zinna, L. Di Bari, N. Zigon and N. Avarvari, *Dalton Trans.*, 2021, **50**, 10533–10539; (*e*) M. Ikeshita, M. Mizugaki, T. Ishikawa, K. Matsudaira, M. Kitahara, Y. Imai and T. Tsuno, *Chem. Commun.*, 2022, **58**, 7503–7506; (*f*) H. Ito, H. Sakai, Y. Okayasu, J. Yuasa, T. Mori and T. Hasobe, *Chem. – Eur. J.*, 2018, **24**, 16889–16894; (*g*) Y. Chen, X. Li, N. Li, Y. Quan, Y. Cheng and Y. Tang, *Mater. Chem. Front.*, 2019, **3**, 867–873.

10 (*a*) Q.-h. Meng, P. Zhou, F. Song, Y.-b. Wang, G.-l. Liu and H. Li, *CrystEngComm*, 2013, **15**, 2786–2790; (*b*) R. Sakamoto, T. Iwashima, J. F. Kogel, S. Kusaka, M. Tsuchiya, Y. Kitagawa and H. Nishihara, *J. Am. Chem. Soc.*, 2016, **138**, 5666–5677; (*c*) A. Gusev, V. Shul'gin, E. Braga, E. Zamnius, G. Starova, K. Lyssenko, I. Eremenko and W. Linert, *J. Lumin.*, 2018, **202**, 370–376; (*d*) A. Gusev, V. Shul'gin, E. Braga, E. Zamnius, M. Kryukova and W. Linert, *Dyes Pigm.*, 2020, **183**, 108626; (*e*) J. Tang, H.-Y. Yin and J.-L. Zhang, *Inorg. Organomet. Transition Met. Complexes Biol. Mol. Living Cells*, 2017, 1–53; (*f*) F. Dumur, E. Contal, G. Wantz and D. Gigmes, *Eur. J. Inorg. Chem.*, 2014, **2014**, 4186–4198; (*g*) A. N. Gusev, M. A. Kiskin, E. V. Braga, M. A. Kryukova, G. V. Baryshnikov, N. N. Karaush-Karmazin, V. A. Minaeva, B. F. Minaev, K. Ivaniuk, P. Stakhira, H. Ågren and W. Linert, *ACS Appl. Electron. Mater.*, 2021, **3**, 3436–3444; (*h*) A. Russegger, L. Eiber, A. Steinegger and S. M. Borisov, *Chemosensors*, 2022, **10**, 91.

11 (*a*) L. Jin, Y. Huang, H. Jing, T. Chang and P. Yan, *Tetrahedron: Asymmetry*, 2008, **19**, 1947–1953; (*b*) F. Meng, Y. Li, W. Zhang, S. Li, Y. Quan and Y. Cheng, *Polym. Chem.*, 2017, **8**, 1555–1561.

12 (*a*) M. Enamullah, G. Makhloufi, R. Ahmed, B. A. Joy, M. A. Islam, D. Padula, H. Hunter, G. Pescitelli and C. Janiak, *Inorg. Chem.*, 2016, **55**, 6449–6464; (*b*) M. Enamullah, M. A. Quddus, M. R. Hasan, G. Pescitelli, R. Berardozzi, G. Makhloufi, V. Vasylyeva and C. Janiak, *Dalton Trans.*, 2016, **45**, 667–680.

13 (*a*) K. Takaishi, S. Hinoide, T. Matsumoto and T. Ema, *J. Am. Chem. Soc.*, 2019, **141**, 11852–11857; (*b*) T. Kimoto, N. Tajima, M. Fujiki and Y. Imai, *Chem. - Asian J.*, 2012, **7**, 2836–2841; (*c*) T. Kimoto, T. Amako, N. Tajima, R. Kuroda, M. Fujiki and Y. Imai, *Asian J. Org. Chem.*, 2013, **2**, 404–410; (*d*) Y. Nojima, M. Hasegawa, N. Hara, Y. Imai and Y. Mazaki, *Chem. Commun.*, 2019, **55**, 2749–2752.

14 M. J. Frisch, G. W. Trucks, H. B. Schlegel, G. E. Scuseria, M. A. Robb, J. R. Cheeseman, G. Scalmani, V. Barone,

G. A. Petersson, H. Nakatsuji, X. Li, M. Caricato, A. V. Marenich, J. Bloino, B. G. Janesko, R. Gomperts, B. Mennucci, H. P. Hratchian, J. V. Ortiz, A. F. Izmaylov, J. L. Sonnenberg, D. Williams-Young, F. Ding, F. Lipparini, F. Egidi, J. Goings, B. Peng, A. Petrone, T. Henderson, D. Ranasinghe, V. G. Zakrzewski, J. Gao, N. Rega, G. Zheng, W. Liang, M. Hada, M. Ehara, K. Toyota, R. Fukuda, J. Hasegawa, M. Ishida, T. Nakajima, Y. Honda, O. Kitao, H. Nakai, T. Vreven, K. Throssell, J. A. Montgomery Jr., J. E. Peralta, F. Ogliaro, M. J. Bearpark, J. J. Heyd, E. N. Brothers, K. N. Kudin, V. N. Staroverov, T. A. Keith, R. Kobayashi, J. Normand, K. Raghavachari, A. P. Rendell, J. C. Burant, S. S. Iyengar, J. Tomasi, M. Cossi, J. M. Millam, M. Klene, C. Adamo, R. Cammi, J. W. Ochterski, R. L. Martin, K. Morokuma, O. Farkas, J. B. Foresman and D. J. Fox, Gaussian, Inc., Wallingford CT, 2016.

15 (*a*) T. Yanai, D. P. Tew and N. C. Handy, *Chem. Phys. Lett.*, 2004, **393**, 51–57; (*b*) A. D. Becke, *J. Chem. Phys.*, 1993, **98**, 5648–5652; (*c*) C. Lee, W. Yang and R. G. Parr, *Phys. Rev. B: Condens. Matter Mater. Phys.*, 1988, **37**, 785–789.

16 V. Barone and M. Cossi, *J. Phys. Chem. A*, 1998, **102**, 1995–2001.

17 (*a*) R. Bauernschmitt and R. Ahlrichs, *Chem. Phys. Lett.*, 1996, **256**, 454–464; (*b*) R. E. Stratmann, G. E. Scuseria and M. J. Frisch, *J. Chem. Phys.*, 1998, **109**, 8218–8224; (*c*) G. Scalmani, M. J. Frisch, B. Mennucci, J. Tomasi, R. Cammi and V. Barone, *J. Chem. Phys.*, 2006, **124**, 94107.